Supplementary Information

for

A ternary AppA–PpsR–DNA complex mediates light-regulation of photosynthesis-related gene expression

Andreas Winkler[1], Udo Heintz[1], Robert Lindner[1], Jochen Reinstein[1], Robert Shoeman[1] & Ilme Schlichting[1]

[1]Department of Biomolecular Mechanisms, Max Planck Institute for Medical Research, Heidelberg, Germany. Correspondence should be addressed to A.W. (Andreas.Winkler@mpimf-heidelberg.mpg.de)

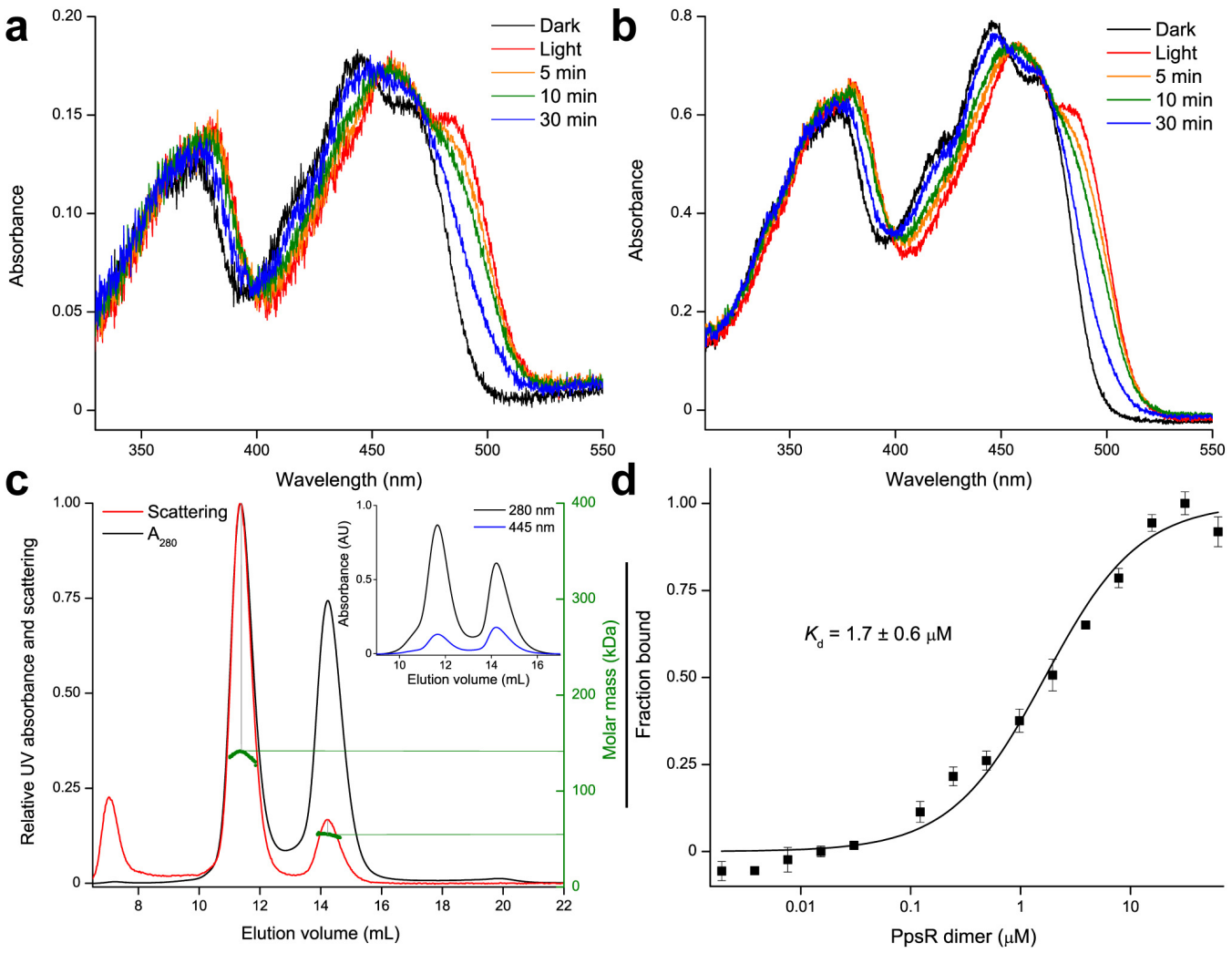

Supplementary Figure 1. Comparison of photocycles of AppA variants and their complex formation with PpsR. (**a**,**b**) Both AppA variants (panel **a** – full-length AppA wild-type and panel **b** –AppA$_{\Delta C}$) are characterized by a 17 nm red-shift in the absorption spectrum upon blue-light absorption. The calculated dark-state recovery rate constants correspond to 5 ± 1 s^{-1} and 6 ± 1 s^{-1} for wild-type and AppA$_{\Delta C}$, respectively (in 10 mM CHES pH 8.5, 500 mM NaCl and 5 % glycerol; 20 °C). Recovery times after illumination of individual traces are provided in the insets. Experimental details are provided in the Supplementary Note. (**c**) Elution profile of PpsR incubated with 2-fold excess of AppA$_{\Delta C}$ on a Superdex 200 10/300 GL column. Static-light scattering detection provided an experimentally determined molecular mass for the complex of 139 ± 5 kDa which agrees well with the theoretical value of 147 kDa (AppA$_{\Delta C}$–PpsR$_2$). The inset shows the UV absorbance traces at 280 and 445 nm. The extracted relative ratios of A_{280}/A_{445} of 6.63 and 3.44 correspond to theoretical values of 6.61 and 3.37 for the AppA$_{\Delta C}$–PpsR$_2$ complex and AppA alone, respectively, confirming the 1:2 stoichiometry[1]. (**d**) Titration of NT–647 labeled full-length AppA C20S with PpsR. Error bars correspond to the standard deviation of MST measurements performed in triplicate. Due to the aggregation tendency of full-length AppA a subtle linear trend overlays the binding curve. This trend is also seen in fluorescence scans of labeled AppA alone but has a negligible effect on the determined K_d of 1.7 μM calculated for a PpsR dimer as binding partner.

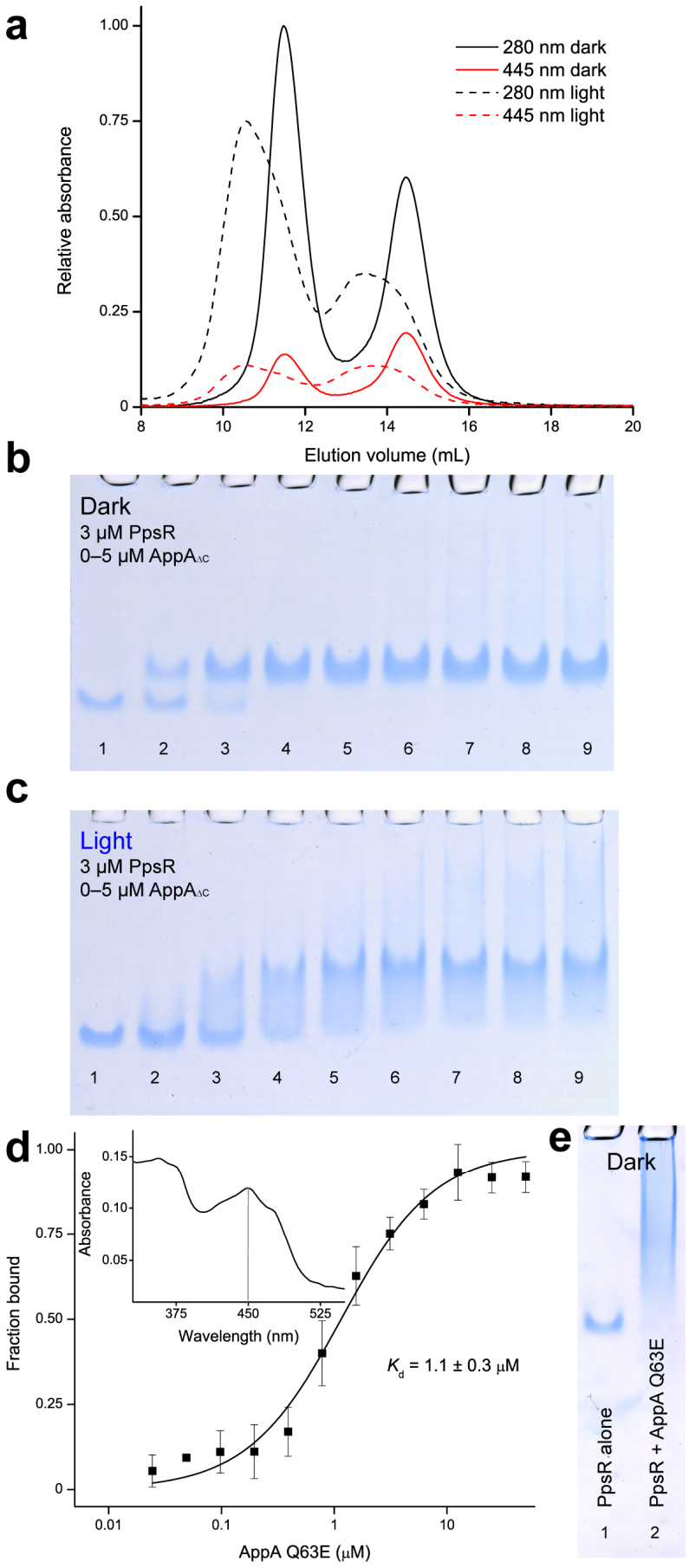
a
1.00
0.75
0.50
0.25
0
Relative absorbance
8
10
12
14
16
18
20
Elution volume (mL)
280 nm dark
445 nm dark
280 nm light
445 nm light
b
Dark
3 μM PpsR
0–5 μM AppA1-112
1 2 3 4 5 6 7 8 9
c
Light
3 μM PpsR
0–5 μM AppA1-112
1 2 3 4 5 6 7 8 9
d
1.00
0.75
0.50
0.25
0
Fraction bound
0.01
0.1
1
10
AppA Q63E (μM)
0.15
0.10
0.05
Absorbance
375
450
525
Wavelength (nm)
Kd = 1.1 ± 0.3 μM
e
Dark
PpsR alone
PpsR + AppA Q63E
1
2

Supplementary Figure 2. Blue-light effect on the binary $AppA_{\Delta C}$–$PpsR_2$ complex. (**a**) Gel fractionation of $AppA_{\Delta C}$–$PpsR_2$ after 15 min incubation of 8 µM $AppA_{\Delta C}$ and PpsR in a total volume of 500 µL in the dark (straight lines, black – 280 nm, red – 445nm). To address the influence of light (dashed lines, same colors) $AppA_{\Delta C}$ was pre-irradiated with blue-light for 5 min at 600 µW cm^{-2} and illumination continued during the incubation time with PpsR. Blue-light irradiation of the gel filtration column was performed throughout the run-time. The observed changes in the elution volume are indicative of structural rearrangements and MALS detection suggested a light-induced dimer formation for $AppA_{\Delta C}$. For the complex species, however, no appreciable change in molar mass was observed. (**b**,**c**) Native PAGE experiments (6 % TGE gels) showing the titration of 3 µM PpsR with increasing concentrations of $AppA_{\Delta C}$ under dark (**b**) and blue-light (**c**) conditions. Semi-quantitative evaluation of the $AppA_{\Delta C}$–$PpsR_2$ complex formation by integration of free PpsR signal intensities in Coomassie-stained gels is presented in Figure 2**a**. The structural change of the complex species indicated in panel **a** can also be seen in the slower migration of the complex species in the illuminated gel. In contrast to PpsR, $AppA_{\Delta C}$ does not form a discrete band in native PAGE but produces a faint smear above the protein complex band. This region also shows substantially retarded mobility upon illumination in line with AppA's light induced conformational change. Lanes 1–9 – 0, 0.75, 1.5, 2.25, 3, 3.5, 4, 4.5, 5 µM $AppA_{\Delta C}$. (**d**) Measurement of the thermophoretic mobility of NT–647 labeled PpsR upon titration with AppA Q63E Δ399 that is locked in the light-activated state[2,3]. A K_d of 1.1 µM, closely resembling that of $AppA_{\Delta C,}$ was obtained after averaging three measurements (error bars correspond to the standard deviation). The inset shows the characteristic partially red-shifted absorbance spectrum of the AppA variant with a maximum at 450 nm (445 nm for wild-type). (**e**) Interaction of PpsR with the light-state locked AppA Q63E variant visualized by native PAGE (6 % TGE). Interestingly, AppA Q63E Δ399 bound to PpsR forms a smeared band on the gel, analogous to the $AppA_{\Delta C}$–$PpsR_2$ complex under blue-light conditions (Supplementary Fig. 3**f**). The increased smearing of this complex species originates from the fact that this gel was run at RT. Lane 1 – 2.8 µM PpsR and lane 2 – 2.8 µM PpsR in the presence of 5 µM AppA Q63E Δ399.

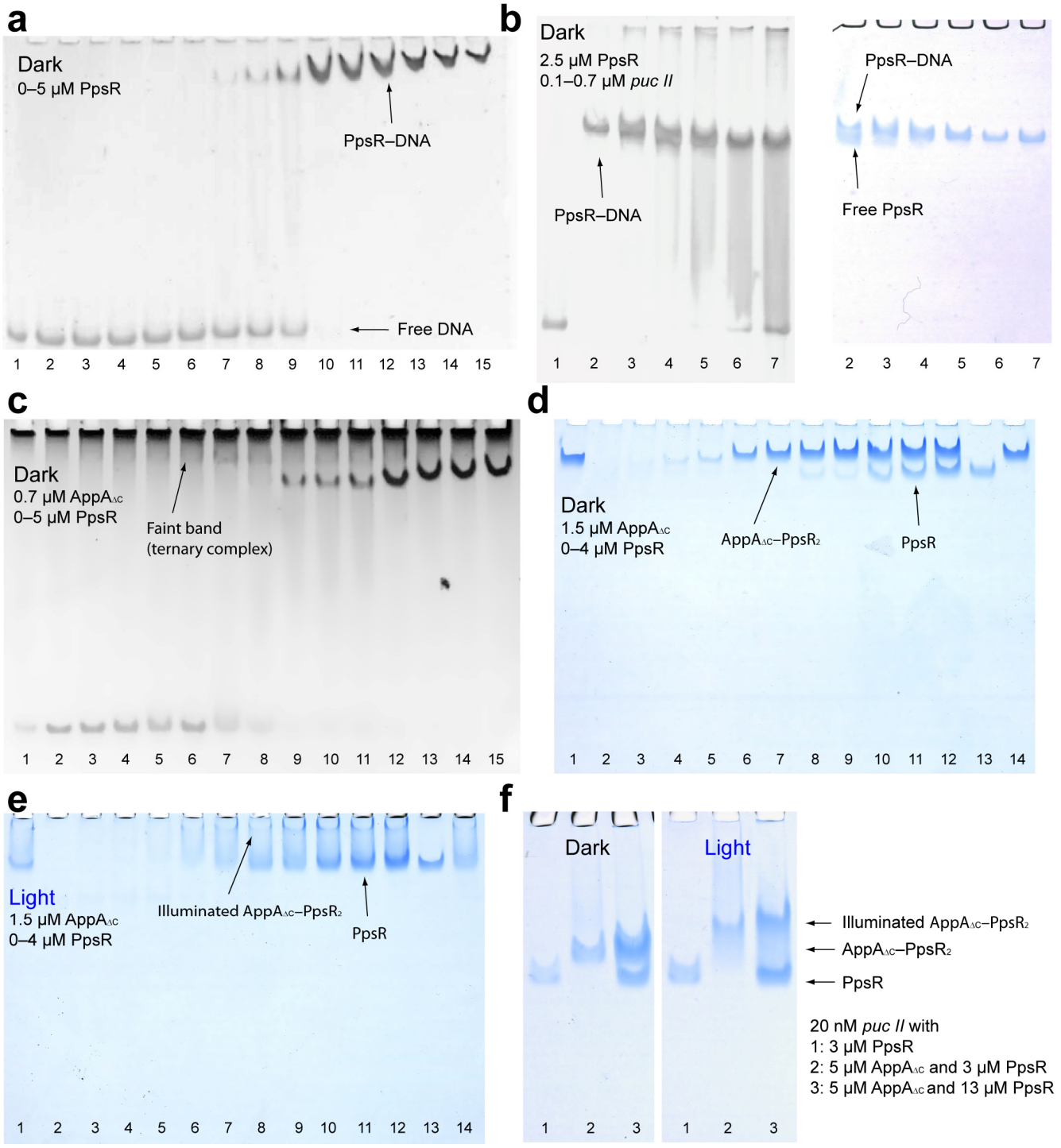

Supplementary Figure 3. Influence of AppA and blue-light on DNA-binding properties of PpsR. (**a**) EMSA showing the titration of 20 nM *puc I* with PpsR on a 10 % TGE gel. Lanes 1–15 – PpsR at 0, 0.03, 0.05, 0.09, 0.15, 0.25, 0.4, 0.6, 0.9, 1.3, 1.7, 2.3, 3.0, 3.8 and 5.0 μM. These data were combined with a finer titration series around the transition point (data not shown). A semi-quantitative evaluation of PpsR affinity is presented in Figure 2**b**. (**b**) DNA (left) and Coomassie stain (right) of a 6 % TGE gel showing the active site titration performed at 2.5 μM PpsR with increasing *puc II* concentrations. Lane 1 – 70 nM *puc II* alone (only shown for the DNA stain), lanes 2–7 – 0.1, 0.2, 0.3, 0.4, 0.5, 0.7 μM *puc II* probe. For the first three titration points a band corresponding to free PpsR is observed in the Coomassie stain below the DNA bound species. At DNA concentrations above 0.3 μM the free DNA probe appears

due to saturation of the 2.5 μM PpsR present indicating a 1:8 stoichiometry of DNA:PpsR. Quantitative analysis of the active site titration is presented in the inset of Figure 2**b**. (**c**) EMSA showing PpsR-titration of 20 nM *puc I* DNA in the presence of 0.7 μM AppA. In addition to DNA bound to PpsR a faint band with slower migration is observed. Lanes 1–15 – PpsR at 0, 0.5, 0.7, 0.9, 1.2, 1.4, 1.6, 1.8, 2.0, 2.2, 2.5, 2.9, 3.4, 4 and 5.0 μM. (**d**) Coomassie stain of the EMSA showing the formation of a ternary $AppA_{\Delta C}$–PpsR–DNA complex upon PpsR titration of 20 nM *puc I* in the presence of 1.5 μM $AppA_{\Delta C}$ (Fig. 2**c**). Excision of the corresponding Coomassie stained bands and peptide mass fingerprinting using MALDI (data not shown) confirmed that the upper DNA-containing band corresponds to a mixture of $AppA_{\Delta C}$ and PpsR while the lower band represents PpsR. Lane 1 – $AppA_{\Delta C}$ + 2 μM PpsR without DNA, Lane 2–12 – 0, 0.1, 0.25, 0.5, 1.0, 1.5, 2.0, 2.5, 3.0, 3.5, 4.0 μM PpsR, lane 13 – 2 μM PpsR without AppA and lane 14 – 2 μM PpsR with $AppA_{\Delta C}$ after 45 min dark recovery of an illuminated sample. (**e**) Coomassie stain of an EMSA showing the influence of blue-light on the ternary $AppA_{\Delta C}$–PpsR–DNA complex upon PpsR-titration of 20 nM *puc I* in the presence of 1.5 μM $AppA_{\Delta C}$ (cf. Fig. 2**d**). The faint upper band reflects the ternary complex and the lower band PpsR. The relative intensities of the two bands are shifted due to the light dependence of the complex affinity (cf. Supplementary Fig. 2**b**,**c**). Lane 1 – AppA + 2 μM PpsR without DNA, Lanes 2–12 – 0, 0.1, 0.25, 0.5, 1.0, 1.5, 2.0, 2.5, 3.0, 3.5, 4.0 μM PpsR, lane 13 – 2 μM PpsR without AppA and lane 14 – sample equivalent to lane 8 after one light-dark cycle. (**f**) Coomassie stain of the EMSA from Figure 2**e** under dark and blue-light conditions using 20 nM of *puc II* probe and $AppA_{\Delta C}$–$PpsR_2$ saturating amounts of $AppA_{\Delta C}$. Lane 1 – 3 μM PpsR, lane 2 – 5 μM $AppA_{\Delta C}$ + 3 μM PpsR and lane 3 – 5 μM $AppA_{\Delta C}$ + 13 μM PpsR (excess).

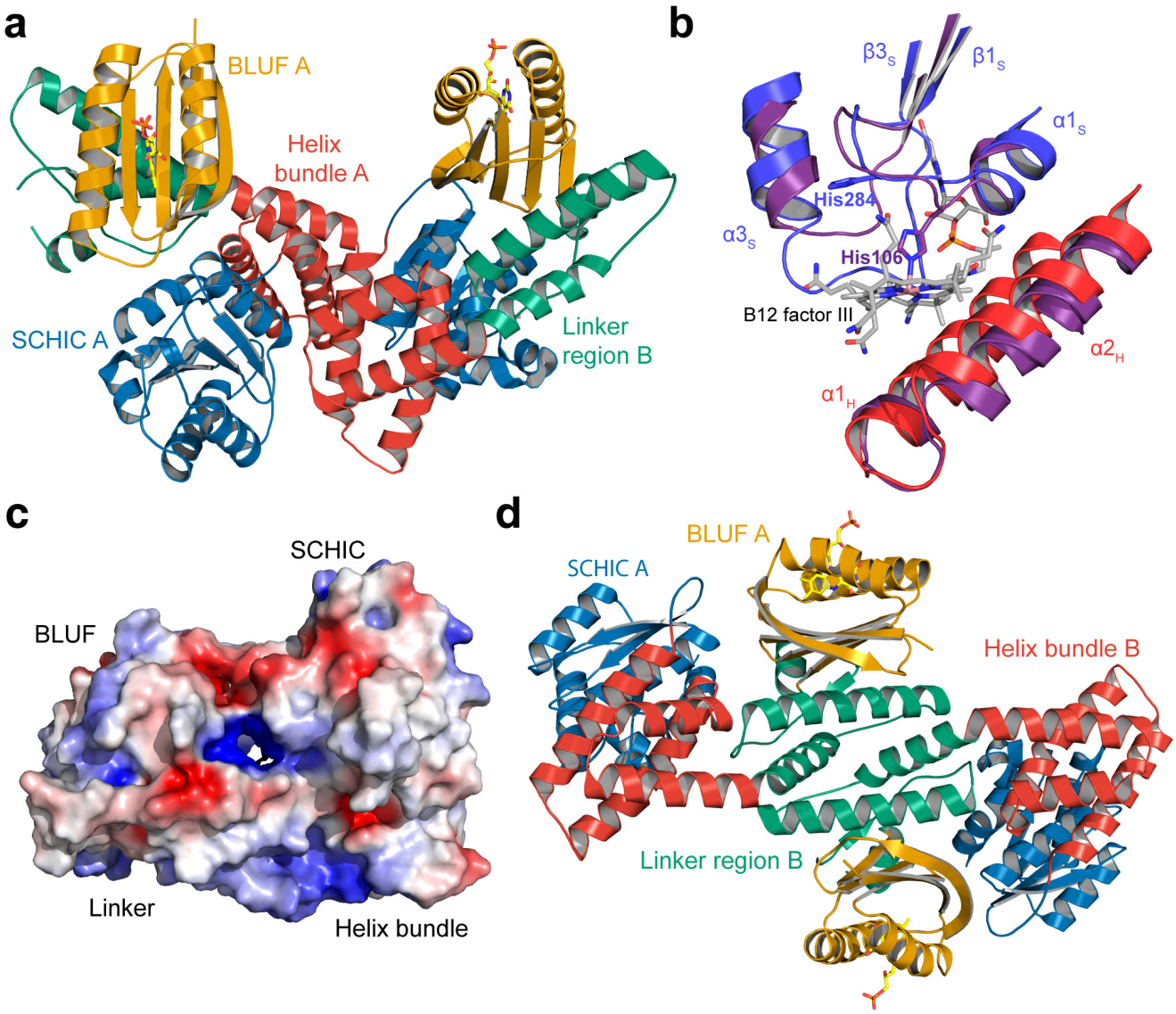

Supplementary Figure 4. Structural details of $AppA_{\Delta C}$. (**a**) Crystal contacts mediated by the 4HB and SCHIC between two protomers of the asymmetric unit in the $AppA_{\Delta C}$ structure. Colors correspond to Figure 3**a**. FMN is shown as yellow stick model. (**b**) Close-up of the SCHIC domain focusing on the B_{12} binding site of evolutionary related corrin binding proteins. His284 in AppA (colored in red and blue for 4HB and SCHIC, respectively) is structurally not related to His106 employed in the coordination of the 5-hydroxybenzimidazolylcobamide cofactor observed in the *Methanosarcina barkeri* monomethylamine corrinoid protein (purple, pdb 3EZX). Based on the conservation of secondary structure elements and the loop between $(\beta1 \text{ and } \alpha1)_{S\_A}$, His284 is shifted by two residues compared to B_{12} binding proteins. (**c**) Surface representation of $AppA_{\Delta C}$. Solvent channels to a cavity between the BLUF and SCHIC domains highlight the weak intramolecular interaction of $AppA_{\Delta C}$ domains. The structure is colored with respect to the electrostatic surface potential showing a random distribution of patches with positive (blue) and negative (red) potentials. (**d**) Crystal contacts mediated by the linker region (bluish-green) of BLUF and 4HB. The protomers of the AppA dimer shown here are related via two-fold crystallographic symmetry. Coloring of individual domains follows Figure 3**a** and FMN is shown as yellow stick model.

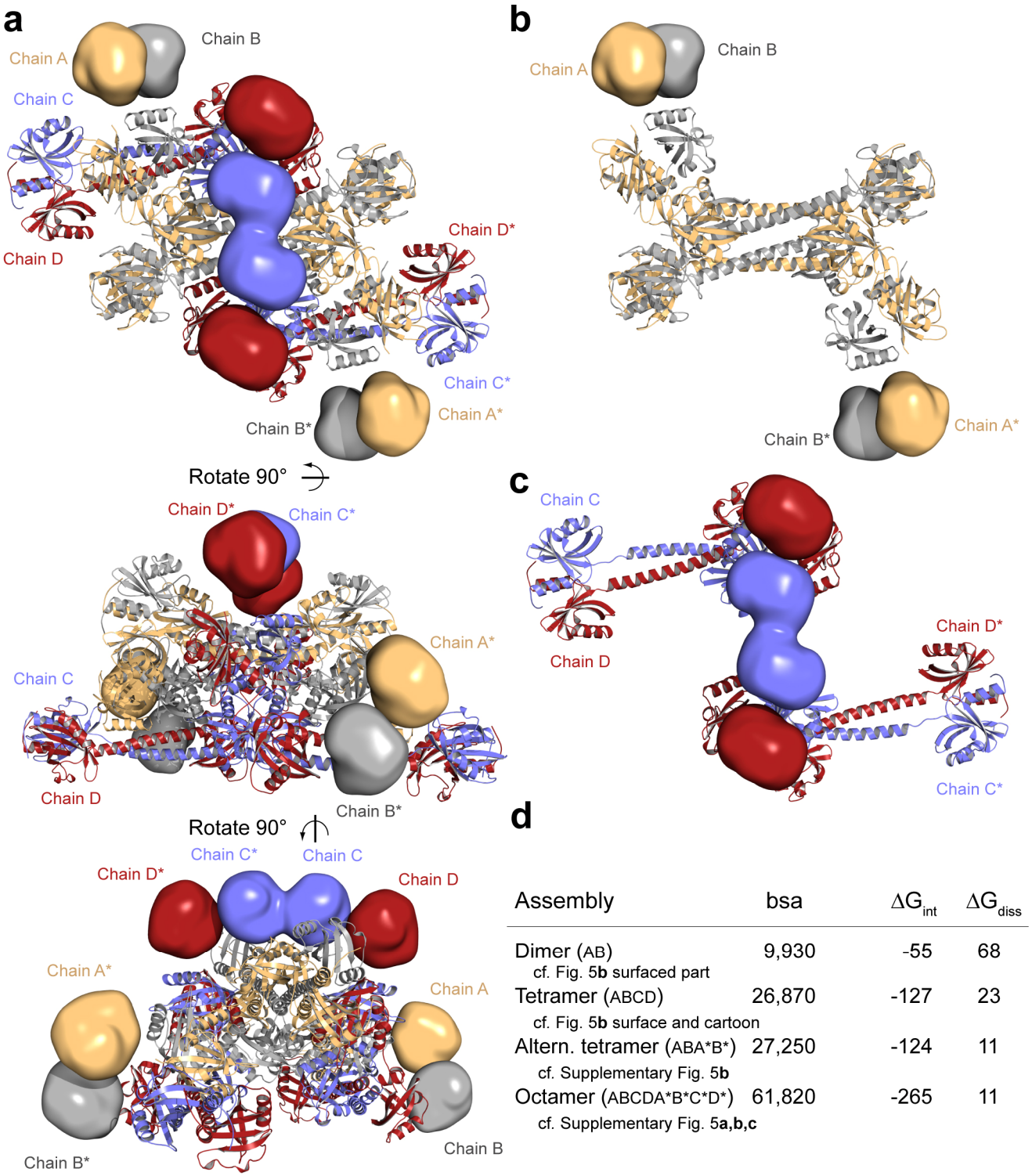

Assembly	bsa	ΔG_{int}	ΔG_{diss}
Dimer (AB) cf. Fig. 5**b** surfaced part	9,930	-55	68
Tetramer (ABCD) cf. Fig. 5**b** surface and cartoon	26,870	-127	23
Altern. tetramer (ABA*B*) cf. Supplementary Fig. 5**b**	27,250	-124	11
Octamer (ABCDA*B*C*D*) cf. Supplementary Fig. 5**a,b,c**	61,820	-265	11

Supplementary Figure 5. Details of oligomer states of PpsR. (**a**) Three 90° rotations of the PpsR ΔHTH octamer are shown in cartoon representation color-coded according to Figure 4**c**. Chains A, B, C and D of the crystallographic symmetry-related tetramer are colored accordingly and marked with an asterisk. The HTH motifs are shown as surface representations extending from the PAS2 C-termini as described in Figure 4**c**. The different orientations highlight the unfavorable distance of two HTH dimers within a single tetrameric unit for DNA-binding without considering major structural rearrangements. Appropriate positioning of four PpsR HTH motifs capable of binding to two palindromes separated by

half a DNA turn in the *puc* promoter depends on the presence of all eight protomers as highlighted in panels **b** and **c**. (**b**) Representation of an alternative PpsR tetramer, mediated solely by the αQ and PAS1 interface equivalent to the octamer interaction. The HTH motifs of this assembly are unlikely to allow efficient DNA-binding, but large structural changes of PAS2 and the HTH motif could occur in this assembly. However, the N–Q–PAS1 construct does not form tetramers at comparable concentrations to full-length PpsR (data not shown) and, in addition, the destabilization of the $\alpha3_{2\_P}$, $\beta4_{2\_P}$ and $\beta5_{2\_P}$ elements observed by HDX upon $AppA_{\Delta C}$–$PpsR_2$ complex formation, supporting a role of the PAS2 domain in tetramerization, favors the Figure 4**b** tetramer as the dominant in-solution assembly of PpsR. (**c**) The four HTH motifs implicated in DNA-binding according to our model (dark-red and light-blue) require the additional four PpsR subunits for proper positioning in the octameric assembly. (**d**) Overview of PISA[4] generated statistics for the individual PpsR oligomers discussed in this study based on the $PpsR_{\Delta HTH}$ structure. High ΔG_{diss} values indicate that a substantial external driving force is necessary to dissociate the corresponding assembly. This clearly highlights PpsR dimers as a stable oligomeric species that can be formed from the less stable tetrameric assembly. The calculated ΔG_{diss} values further favor the crystallographic tetramer (Fig. 4**b**) compared to the alternative tetramer (panel **b**) as the major in-solution species. In full-length PpsR the stability of the octameric assembly would be increased by the additional interaction of the HTH-motifs, especially in the presence of DNA according to the model proposed in Figure 4**c**. bsa – buried surface area ($Å^2$); ΔG_{int} – solvation free energy gain upon formation of the assembly (kcal M^{-1}), ΔG_{diss} – free energy of assembly dissociation (kcal M^{-1}).

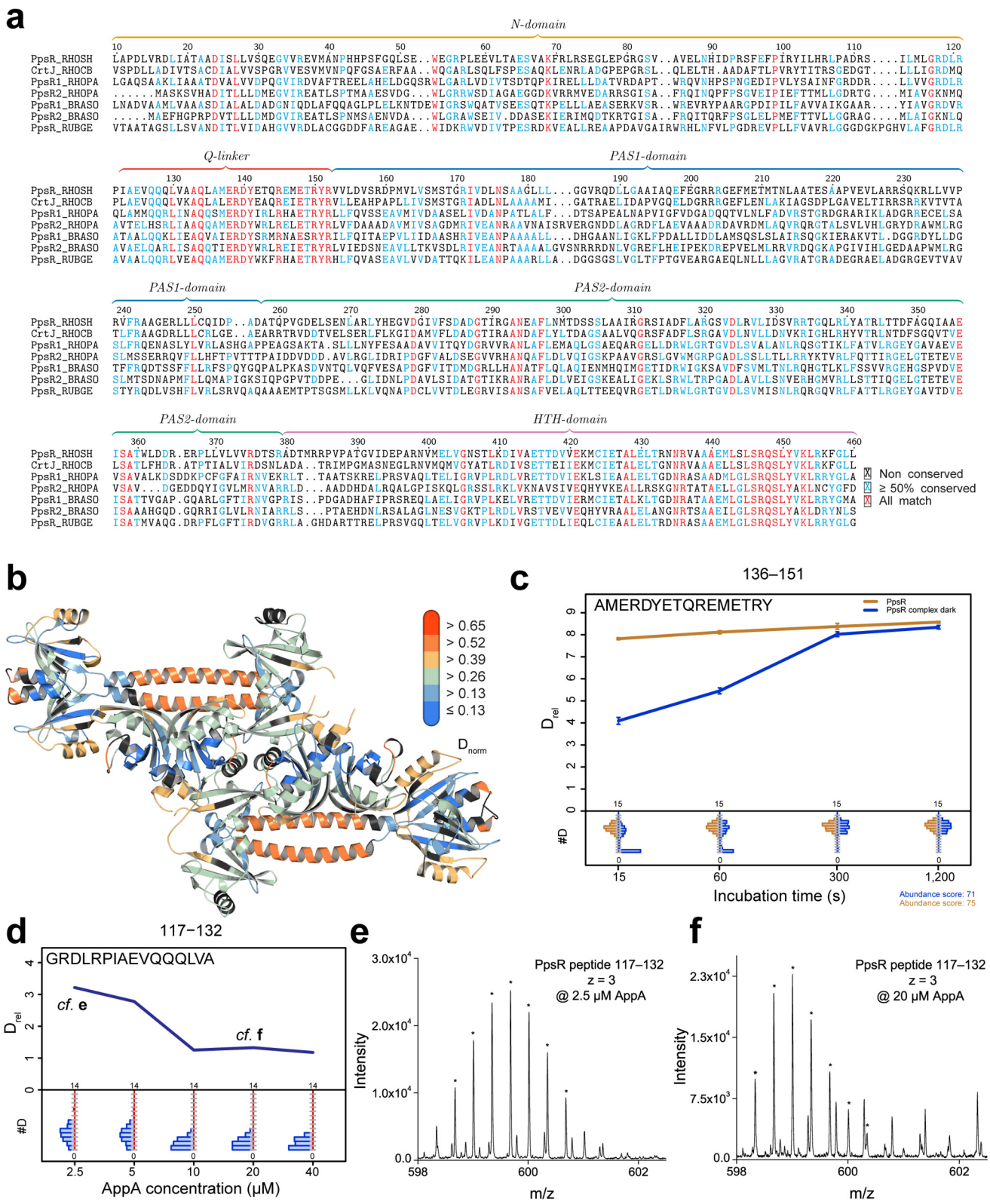

Supplementary Figure 6. Alignment of PpsR homologues and details of HDX experiments for PpsR. (**a**) Multiple sequence alignment of PpsR from different organisms. RHOSH – *R. sphaeroides*, Uniprot accession number (UAN) Q9S301, RHOCB – *R. capsulatus*, UAN D5ANS9, RHOPA – *Rhodopseudomonas palustris* UAN Q6N9L3 and Q6N9K7, BRASO – *Bradyrhizobium sp*. UAN Q6A567 and Q8VUB5, RUBGE – *Rubrivivax gelatinosus* UAN Q9JP99. The alignment was performed

using Jalview and the MUSCLE algorithm[5,6]. (**b**) PpsR structure colored with respect to deuterium incorporation in the dark after 15 sec labeling. Blue colors reflect stable secondary structure elements and the exchange kinetics of regions increase via green to orange and red. The relatively high deuterium incorporation in the Q-linker region reflects the dimer–tetramer equilibrium of PpsR in solution with the Q-linker serving as the docking site for PAS2 domains from the respective other dimer. Details for the normalization procedure (D_{norm}) are described in the Supplementary Note. (**c**) Deuterium uptake plots of a Q-linker peptide in PpsR alone (brown) compared to the $AppA_{\Delta C}$ complexed form (blue). The main sub-panel shows D_{rel} plotted against labeling time for the peptide specified at the top. The estimated abundance distribution of individual deuterated species is presented in the lower sub-panel on a scale from undeuterated (0) to all exchangeable amides deuterated (number of amino acids – prolines – 1). The pronounced protection of αQ upon complex formation with $AppA_{\Delta C}$ features a bimodal distribution of deuterated species as shown in the lower part of the panel. This can be attributed to slower association or dissociation kinetics of the $AppA_{\Delta C}$–$PpsR_2$ complex compared to the chemical exchange rate of free PpsR in this region. This is further supported by an additional non-overlapping αQ peptide as shown in panel **d**. High and stable abundance scores (normalized intensity distribution from 0 to 100 %) for both measurements attest that this observation is not due to carry-over from previous injections. (**d**) $AppA_{\Delta C}$ titration curve for a Q-linker peptide determined by HDX-MS. The main sub-panel shows D_{rel} plotted against $AppA_{\Delta C}$ concentration for the peptide specified at the top. A software estimated abundance distribution of individual deuterated species is presented in the lower sub-panel on a scale from undeuterated (0) to all exchangeable amides deuterated. 10 μM $AppA_{\Delta C}$ corresponds to the concentration used in the full datasets evaluated and described in this work. Additional experiments were performed at constant PpsR concentrations and the indicated $AppA_{\Delta C}$ concentrations during labeling. Deuterium incorporation after 15 s labeling is shown for all concentrations. EX1-like exchange characteristics are supported by the increased distribution width during the transition from free PpsR to $AppA_{\Delta C}$–$PpsR_2$. (**e**,**f**) Raw data corresponding to 15 s labeling time and the 2.5 and 20 μM $AppA_{\Delta C}$ titration points of the peptide shown in panel **d**. The seven most intense isotope peaks of the series of interest are marked with an asterisk.

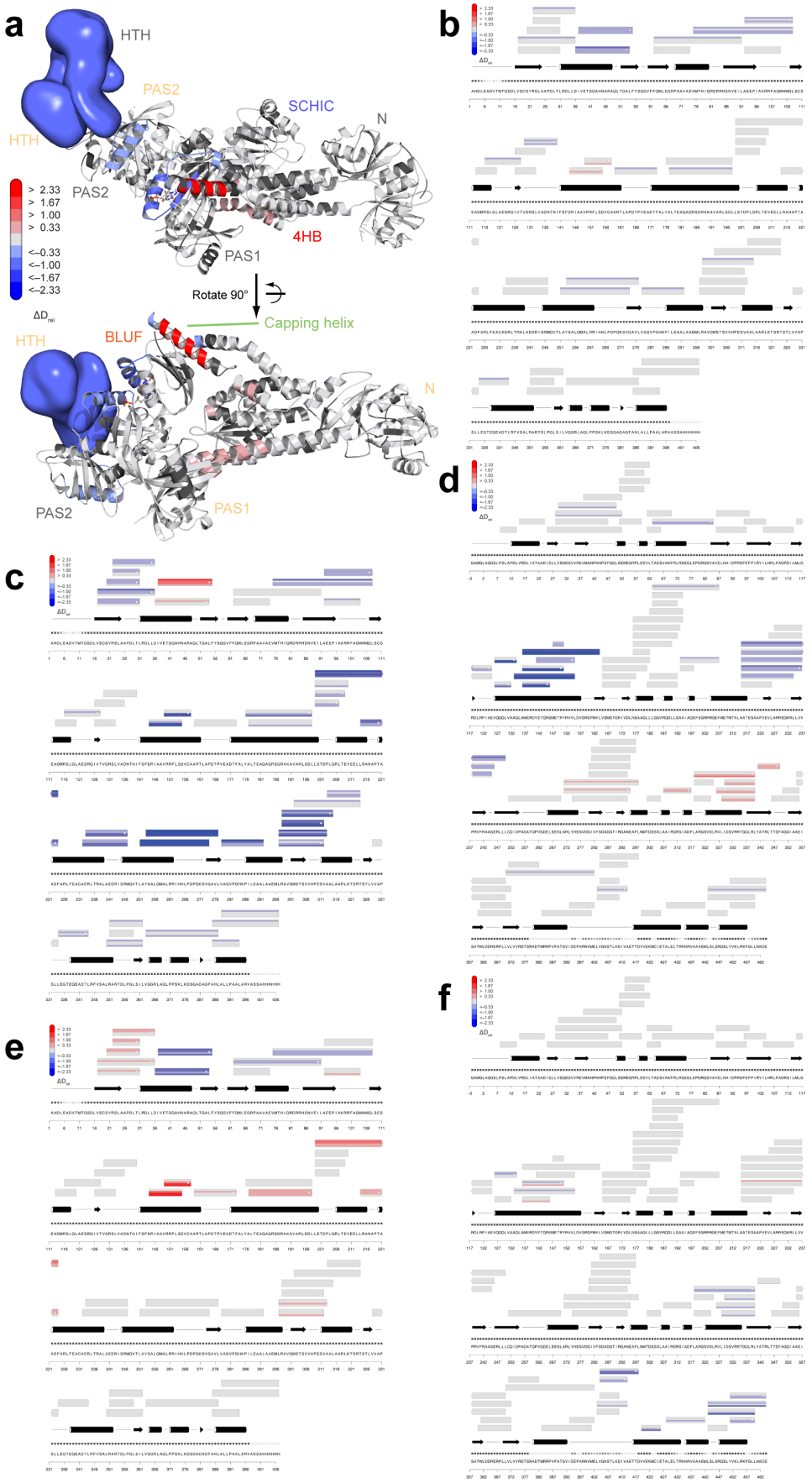
a
HTH
PAS2
SCHIC
N
HTH
PAS2
4HB
PAS1
> 2.33
> 1.67
> 1.00
> 0.33
<–0.33
<–1.00
<–1.67
<–2.33
ΔDrel
Rotate 90°
Capping helix
HTH
BLUF
N
PAS2
PAS1
b
c
d
e
f

Supplementary Figure 7. Summary of HDX experiments. (**a**) The model of the $AppA_{\Delta C}$–$PpsR_2$ complex as described in Figure 6c colored with respect to the observed changes in deuterium incorporation between light- and dark-state measurements of the complex. The 15 s time point is shown for visualization of protection (blue) or destabilization (red) upon complex illumination. See also Supplementary Movie 7 for the full time dependence. The color of the HTH-blob models corresponds to an averaged value for all peptides originating from this region. A complete illustration of all AppA and PpsR peptides evaluated by HDX in the various analyzed states is presented in panels **b**-**f**. Zoom in on the electronic version to reveal full details, with each box reflecting one peptide and containing up to four different colors that, from the bottom up, represent the incubation times of 15, 60, 300 and 1,200 s, respectively. Individual colors correspond to the change in relative deuteration (ΔD_{rel}) of the two compared states according to the legend in the top left corner. MS^2 confirmed peptides are marked with diamonds. Terminal arrows at the end of a box indicate continuation of the peptide in the previous or following line. Secondary structure elements are taken from DSSP analysis[7] of the corresponding structures. Numbering corresponds to the wild-type proteins (Uniprot Q53119 for AppA and Q9S301 for PpsR). In addition, a compilation of all deuteration plots for $AppA_{\Delta C}$ and PpsR can be found in Supplementary Figure 8. (**b**) Changes in $AppA_{\Delta C}$ deuteration upon blue-light illumination (also see Supplementary Movie 1). (**c**) Changes in $AppA_{\Delta C}$ deuteration upon complex formation with PpsR (also see Supplementary Movies 2 and 6). (**d**) Changes in deuteration of PpsR upon complex formation with $AppA_{\Delta C}$ (also see Supplementary Movies 3 and 6). (**e**) Changes in $AppA_{\Delta C}$ deuteration upon blue-light illumination of the complex species (also see Supplementary Movies 4 and 7). (**f**) Changes in deuteration of PpsR upon blue-light illumination of $AppA_{\Delta C}$–$PpsR_2$ (also see Supplementary Movies 5 and 7).

a

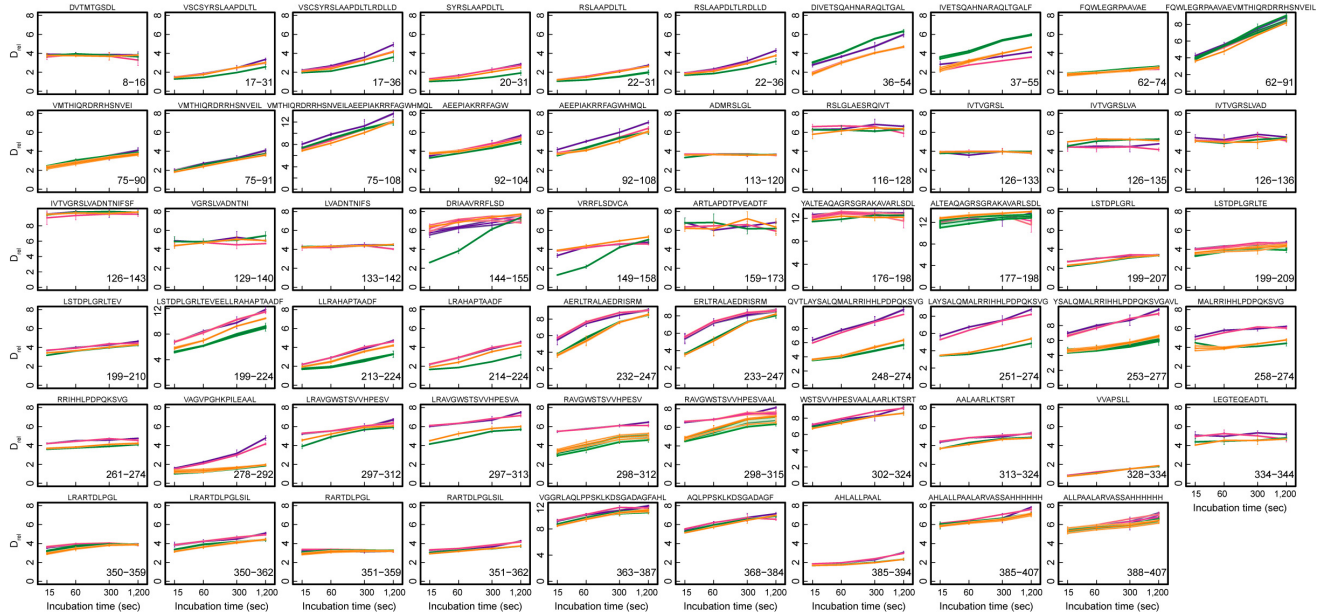
DVTMTGSDL
8–16
VSCSYRSLAAPDLTL
17–31
VSCSYRSLAAPDLTLRDLLD
17–36
SYRSLAAPDLTL
20–31
RSLAAPDLTL
22–31
RSLAAPDLTLRDLLD
22–36
DIVETSQAHNARAQLTGAL
36–54
IVETSQAHNARAQLTGALF
37–55
FQWLEGRPAAVAE
62–74
FQWLEGRPAAVAEVMTHIQRDRRHSNVEIL
62–91
VMTHIQRDRRHSNVEI
75–90
VMTHIQRDRRHSNVEILAEEPIAKRRFAGWHMQL
75–91
VMTHQRDRRHSNVEILAEEPIAKRRFAGWHMQL
75–108
AEEPIAKRRFAGW
92–104
AEEPIAKRRFAGWHMQL
92–108
ADMRSLGL
113–120
RSLGLAESRQIVT
116–128
IVTVGRSL
126–133
IVTVGRSLVA
126–135
IVTVGRSLVAD
126–136
IVTVGRSLVADNTNIFSF
126–143
VGRSLVADNTNI
129–140
LVADNTNIFS
133–142
DRIAAVRRFLSD
144–155
VRRFLSDVCA
149–158
ARTLAPDTPVEADTF
159–173
YALTEAQAGRSGRAKAVARLSDL
176–198
ALTEAQAGRSGRAKAVARLSDL
177–198
LSTDPLGRL
199–207
LSTDPLGRLTE
199–209
LSTDPLGRLTEV
199–210
LSTDPLGRLTEVEELLRAHAPTAADF
199–224
LLRAHAPTAADF
213–224
LRAHAPTAADF
214–224
AERLTRALAEDRISRM
232–247
ERLTRALAEDRISRM
233–247
QVTLAYSALQMALRRIHHLPDPQKSVG
248–274
LAYSALQMALRRIHHLPDPQKSVG
251–274
YSALQMALRRIHHLPDPQKSVGAVL
253–277
MALRRIHHLPDPQKSVG
258–274
RRIHHLPDPQKSVG
261–274
VAGVPGHKPILEAAL
278–292
LRAVGWSTSVVHPESV
297–312
LRAVGWSTSVVHPESVA
297–313
RAVGWSTSVVHPESV
298–312
RAVGWSTSVVHPESVAAL
298–315
WSTSVVHPESVAALAARLKTSRT
302–324
AALAARLKTSRT
313–324
VVAPSLL
328–334
LEGTEQEADTL
334–344
LRARTDLPGL
350–359
LRARTDLPGLSIL
350–362
RARTDLPGL
351–359
RARTDLPGLSIL
351–362
VGGRLAQLPPSKLKDSGADAGFAHL
363–387
AQLPPSKLKDSGADAGF
368–384
AHLALLPAAL
385–394
AHLALLPAALARVASSAHHHHHH
385–407
ALLPAALARVASSAHHHHHH
388–407
Dwt
Incubation time (sec)
15
60
300
1,200

b

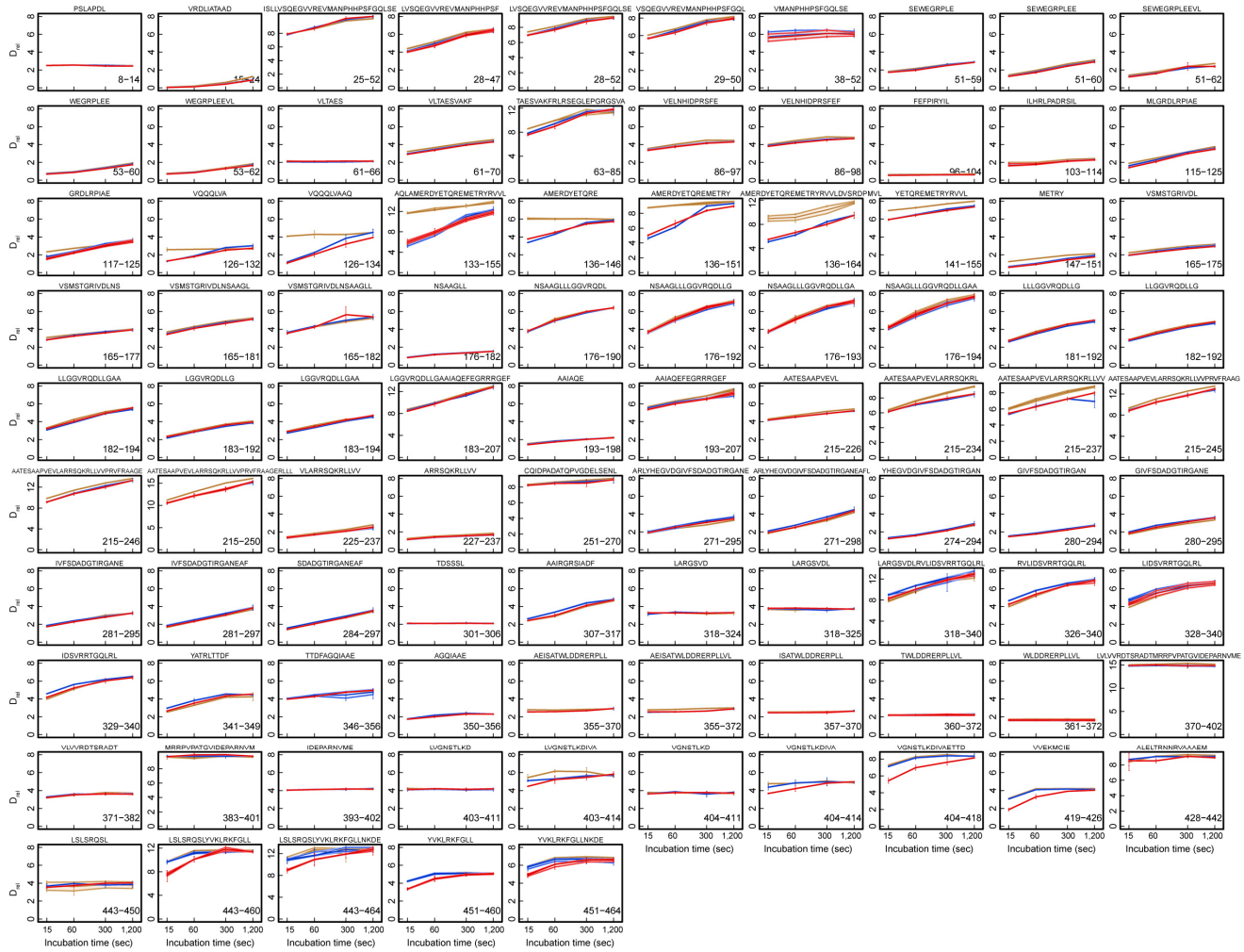
PSLAPDL
8–14
VRDLIATAAD
15–24
ISLLVSQEGVVREVMANPHHPSFGQLSE
25–52
LVSQEGVVREVMANPHHPSF
28–47
LVSQEGVVREVMANPHHPSFGQLSE
28–52
VSQEGVVREVMANPHHPSFGQL
29–50
VMANPHHPSFGQLSE
38–52
SEWEGRPLE
51–59
SEWEGRPLEE
51–60
SEWEGRPLEEVL
51–62
WEGRPLEE
53–60
WEGRPLEEVL
53–62
VLTAES
61–66
VLTAESVAKF
61–70
TAESVAKFRLRSEGLEPGRGSVA
63–85
VELNHIDPRSFE
86–97
VELNHIDPRSFEF
86–98
FEFPIRYIL
96–104
ILHRLPADRSIL
103–114
MLGRDLRPIAE
115–125
GRDLRPIAE
117–125
VQQQLVA
126–132
VQQQLVAAQ
126–134
AQLAMERDYETQREMETRYRVVL
133–155
AMERDYETQRE
136–146
AMERDYETQREMETRY
136–151
AMERDYETQREMETRYRVVLDVSRDPMVL
136–164
YETQREMETRYRVVL
141–155
METRY
147–151
VSMSTGRIVDL
165–175
VSMSTGRIVDLNS
165–177
VSMSTGRIVDLNSAAGL
165–181
VSMSTGRIVDLNSAAGLL
165–182
NSAAGLL
176–182
NSAAGLLLGGVRQDL
176–190
NSAAGLLLGGVRQDLLG
176–192
NSAAGLLLGGVRQDLLGA
176–193
NSAAGLLLGGVRQDLLGAA
176–194
LLLGGVRQDLLG
181–192
LLGGVRQDLLG
182–192
LLGGVRQDLLGAA
182–194
LGGVRQDLLG
183–192
LGGVRQDLLGAA
183–194
LGGVRQDLLGAAIAQEFEGRRRGEF
183–207
AAIAQE
193–198
AAIAQEFEGRRRGEF
193–207
AATESAAPVEVL
215–226
AATESAAPVEVLARRSQKRL
215–234
AATESAAPVEVLARRSQKRLLVV
215–237
AATESAAPVEVLARRSQKRLLVVPRVFRAAG
215–245
AATESAAPVEVLARRSQKRLLVVPRVFRAAGERLLL
215–246
AATESAAPVEVLARRSQKRLLVVPRVFRAAGERLLL
215–250
VLARRSQKRLLVV
225–237
ARRSQKRLLVV
227–237
CQIDPADATQPVGDELSENL
251–270
ARLYHEGVDGIVFSDADGTIRGANE
271–295
ARLYHEGVDGIVFSDADGTIRGANEAFL
271–298
YHEGVDGIVFSDADGTIRGAN
274–294
GIVFSDADGTIRGAN
280–294
GIVFSDADGTIRGANE
280–295
IVFSDADGTIRGANE
281–295
IVFSDADGTIRGANEAF
281–297
SDADGTIRGANEAF
284–297
TDSSSL
301–306
AAIRGRSIADF
307–317
LARGSVD
318–324
LARGSVDL
318–325
LARGSVDLRVLIDSVRRTGQLRL
318–340
RVLIDSVRRTGQLRL
326–340
LIDSVRRTGQLRL
328–340
IDSVRRTGQLRL
329–340
YATRLTTDF
341–349
TTDFAGQIAAE
346–356
AGQIAAE
350–356
AEISATWLDDRERPLL
355–370
AEISATWLDDRERPLLVL
355–372
ISATWLDDRERPLL
357–370
TWLDDRERPLLVL
360–372
WLDDRERPLLVL
361–372
LVLVVRDTSRADTMRRPVPATGVIDEPARNVME
370–402
VLVVRDTSRADT
371–382
MRRPVPATGVIDEPARNVM
383–401
IDEPARNVME
393–402
LVGNSTLKD
403–411
LVGNSTLKDIVA
403–414
VGNSTLKD
404–411
VGNSTLKDIVA
404–414
VGNSTLKDIVAETTD
404–418
VVEKMCIE
419–426
ALELTRNNRVAAAEM
428–442
LSLSRQSL
443–450
LSLSRQSLVVKLRKFGLL
443–460
LSLSRQSLYVKLRKFGLLNKDE
443–464
YVKLRKFGLL
451–460
YVKLRKFGLLNKDE
451–464
Dwt
Incubation time (sec)
15
60
300
1,200

Supplementary Figure 8. Individual deuterium incorporation plots of all evaluated peptides. (**a**) $AppA_{\Delta C}$ traces are colored in purple, pink, green and orange corresponding to free $AppA_{\Delta C}$ in the dark- and light-state, as well as $AppA_{\Delta C}$–$PpsR_2$ in the dark- and light-state, respectively. (**b**) PpsR traces colored in brown, blue and red correspond to free PpsR, as well as $AppA_{\Delta C}$–$PpsR_2$ in the dark- and light-state, respectively. Peptide sequences and their corresponding numbers are shown on top and in the bottom right corner, respectively, of each sub-panel. Ordinates of each plot correspond to the relative deuterium incorporation and abscissae to the labeling time in seconds, shown at the bottom of each panel. Zoom in on the figure in the electronic version for full details.

Supplementary Table 1. List of primers for generation of different AppA and PpsR constructs and for amplification of DNA probes for EMSAs.

Primer	Description	Sequence 5′ to 3′
1	AppA forward (fw.)	GCTACCATGGCGCACGACCTCGAGGCGGACG
2	AppA full reverse (rv.)	TATGCGGCCGCTCAGTGATGGTGATGGTGATGGGCGCTG GCGCTGCGGCGGCGGTC
3	AppA Δ399 rv.	TATGCGGCCGCTCAGTGATGGTGATGGTGATGGGCGCTGC TGGCCACACGGGCGAGGGC
4	AppA 4HB-SCHIC fw.	TACGCCATGGTCGAGGCGGACACCTTCGC
5	C20S mutagenesis fw.	GATCTGGTTTCCTGCTCCTACCGCAGCCTGGCG
6	C20S mutagenesis rv.	CGCCAGGCTGCGGTAGGAGCAGGAAACCAGATC
7	Q63E mutagenesis fw.	GCCAGGGCGTCTTCTTCGAATGGCTCGAAGGCCGCC
8	Q63E mutagenesis rv.	GGCGGCCTTCGAGCCATTCGAAGAAGACGCCCTGGC
9	PpsR fw.	ATATCCATGGGAATGGGTCTGGCAGGCGGTTC
10	PpsR full rv.	ATATGCGGCCGCCTCGAGTTATTCATCTTTATTCAGCAGG
11	PpsR ΔHTH rv.	ATATGCGGCCGCTTAACGGCTGGTATCACGAACAACC
12	PpsR N–Q–PAS1 rv.	ATATGCGGCCGCTTAATCTGCCGGATCAATCTGACACAGC
13	*puc I* fw.	Cy5-ATCCAAAACGGCCTTGTC
14	*puc I* rv.	ATCGCATTATGGGTGTCAC
15	*puc II* fw.	Cy5-GGACAGGCAGCGTCAATTTC
16	*puc II* rv.	TTGCGTGTAGGGCCTGCACG

Supplementary Movie 1. Animation of differential plots showing evaluated peptides from two HDX experiments ($AppA_{\Delta C,light}$ – $AppA_{\Delta C,dark}$) plotted onto the structure of $AppA_{\Delta C}$. Colors correspond to the bar legend in the animation with red indicating increased deuterium uptake in the light-state measurement of isolated $AppA_{\Delta C}$. The time course represents the deuterium labeling times of 15, 60, 300 and 1,200 seconds. See Supplementary Figure 7**b** for details of peptides used in this animation with additional overlapping peptides supporting the colors in this movie.

Supplementary Movie 2. Animation of differential plots showing evaluated peptides from two HDX experiments [($AppA_{\Delta C}$–$PpsR_{2,dark}$) – $AppA_{\Delta C,dark}$] plotted onto the structure of $AppA_{\Delta C}$. Colors correspond to the bar legend in the animation with blue indicating reduced deuterium uptake upon complex formation. The time course corresponds to the deuterium labeling times of 15, 60, 300 and 1,200 seconds. See Supplementary Figure 7**c** for details of peptides used in this animation with additional overlapping peptides supporting the colors in this movie.

Supplementary Movie 3. Animation of differential plots showing evaluated peptides from two HDX experiments [($AppA_{\Delta C}$–$PpsR_{2,dark}$) – $PpsR_{dark}$] plotted onto the $PpsR_{\Delta HTH}$ structure. Colors correspond to the bar legend in the animation with blue indicating reduced deuterium uptake upon complex formation. The time course corresponds to the deuterium labeling times of 15, 60, 300 and 1,200 seconds. See Supplementary Figure 7**d** for details of peptides used in this animation with additional overlapping peptides supporting the colors in this movie.

Supplementary Movie 4. Animation of differential plots of evaluated peptides from two HDX experiments [($AppA_{\Delta C}$–$PpsR_{2,light}$) – ($AppA_{\Delta C}$–$PpsR_{2,dark}$)] plotted onto the structure of $AppA_{\Delta C}$. Colors correspond to the bar legend in the animation with red indicating increased deuterium uptake in the light-state measurement of the complex. The time course represents the deuterium labeling times of 15, 60, 300 and 1,200 seconds. See Supplementary Figure 7**e** for details of peptides used in this animation with additional overlapping peptides supporting the colors in this movie.

Supplementary Movie 5. Animation of differential plots showing evaluated peptides from two HDX experiments [($AppA_{\Delta C}$–$PpsR_{2,light}$) – ($AppA_{\Delta C}$–$PpsR_{2,dark}$)] plotted onto the $PpsR_{\Delta HTH}$ structure. Colors correspond to the bar legend in the animation with red indicating increased deuterium uptake in the light-state measurement of the complex. The subtle destabilization observed for some αQ peptides originates from peptides exhibiting EX1-like deuteration characteristics and can therefore be attributed to the slightly lower affinity of the complex species during labeling under light conditions, as suggested by the native PAGE data. The time course represents the deuterium labeling times of 15, 60, 300 and 1,200 seconds. See Supplementary Figure 7**f** for details of peptides used in this animation with additional overlapping peptides supporting the colors in this movie.

Supplementary Movie 6. Animation of differential plots showing evaluated peptides from three HDX experiments [($AppA_{\Delta C}$–$PpsR_{2,dark}$) – $PpsR_{dark}$] and [($AppA_{\Delta C}$–$PpsR_{2,dark}$) – $AppA_{\Delta C,dark}$] plotted onto the structures of the PpsR and AppA subunits of the core complex, respectively. Colors correspond to the bar legend in the animation with blue indicating reduced deuterium uptake upon complex formation. The time course corresponds to the deuterium labeling times of 15, 60, 300 and 1,200 seconds.

Supplementary Movie 7. Animation of differential plots showing evaluated peptides from two HDX experiments [($AppA_{\Delta C}$–$PpsR_{2,light}$) – ($AppA_{\Delta C}$–$PpsR_{2,dark}$)] plotted onto a full length model of the $AppA_{\Delta C}$–$PpsR_2$ complex structure generated as described for Figure 6**c**. The blobs representing the HTH dimer are colored with an average color for the peptides originating from this region. Colors correspond to the bar legend in the animation with blue indicating reduced deuterium uptake upon complex illumination. The time course corresponds to the deuterium labeling times of 15, 60, 300 and 1,200 seconds.

Supplementary Note

Microscale thermophoresis

We quantified the interaction of AppA and PpsR using microscale thermophoresis (Nanotemper). For this purpose, we labeled either PpsR or AppA constructs at the amine positions using the NHS-reactive dye NT–647 (Nanotemper) according to the instructions of the manufacturer. Titrations with the labeled species kept constant and varying the corresponding other protein concentration in 1:2 dilutions over an appropriate concentration range were carried out in buffer B. We used standard treated capillaries (Nanotemper) for all experiments. Data of three individual experiments were evaluated using the quadratic equation of the law of mass action for fitting with a fixed concentration of the labeled species. Protein concentrations were quantified by their absorption at 280 nm (see below).

AppA control experiments addressing the truncation and mutation

Low expression levels of soluble AppA and a tendency of the protein to aggregate have hampered its analysis in the past[1,8,9]. Deletion of the cysteine-rich region resulted in five-fold higher yields of soluble protein with the shortened construct, termed AppA Δ399. The yield can be further improved ten-fold by mutating Cys20 to serine. Together, these modifications enabled purification of AppA in the quantities and quality needed for a detailed biochemical and biophysical characterization.

Control experiments shown in Supplementary Figure 1**a**,**b**,**c**,**d** confirm that neither the BLUF photocycle nor AppA–$PpsR_2$ complex formation is affected by the C20S mutation and the C-terminal truncation of AppA. In addition, the functionality of AppA lacking the cysteine-rich region has been shown *in vivo*[10]. For this reason, if not indicated otherwise, all experiments were performed with the AppA Δ399 C20S construct which is referred to as $AppA_{\Delta C}$.

Structural aspects of the AppA SCHIC domain

The 4HB and SCHIC arrangement resembles combinations of helix bundles with the evolutionary related corrinoid binding domains (SCOP 52242), respectively (e.g. pdb 3EZX). The second pair of helices from the 4HB interacts with the SCHIC domain and forms a hydrophobic interface where the B12 cofactor would be located in the case of corrinoid binding proteins. In our structure no cofactor is bound since we performed expression and purification under aerobic conditions, where the proposed heme ligand for this domain does not co-purify[9,10]. Notably, His284 positioned in the loop between β1 and α1 of the SCHIC domain, was previously suggested as axial ligand for cofactor binding[10,11]. However, it is structurally unrelated to the histidine involved in B12 binding (Supplementary Fig. 4**b**).

HDX-MS

HDX was used to address complex formation and light-induced structural rearrangements in AppA and PpsR. Incubation in D_2O containing buffer was carried out for various times under dark or blue-light conditions and allowed measuring the time dependent deuterium uptake in amide positions at an average resolution of several amino acids. The observed exchange characteristics provide information on the stability and dynamics of the secondary structure elements since these affect deuterium uptake. Quantification of the absolute deuterium uptake requires measurement of the back-exchange rates for individual peptides (~35 % at our experimental conditions); however, comparative experiments performed under identical experimental conditions for two different conformations of a protein enable the interpretation in terms of structural changes between the two states without quantitative back-exchange determination[11].

In contrast to comparative experiments, the colors used in Figure 3**d** and Supplementary Figure 6**b** indicate the average deuterium incorporation from a single HDX experiment. While blue regions describe elements incorporating less than average deuterium per amide position and hence reflect stable secondary structure elements, the degree of exchange increases from green to orange to red. Interestingly, the higher average deuterium incorporation in the linker region of $AppA_{\Delta C}$ is mainly caused by peptides reaching their highest deuteration level already upon short deuterium exposure. This indicates a significant fraction of unstructured or flexible elements. Therefore, the conformation of the linker region as observed in the crystal structure needs careful interpretation, particularly as the linker forms crystal contacts with a symmetry related molecule (Supplementary Fig. 4**d**).

We initially analyzed deuterium incorporation manually in a semi-automated process using HX-Express[12] and used the obtained results for quality control of data generated by an improved version of the automated software package Hexicon[13]. This in-house developed program (to be published) is based on the previously published NITPICK algorithm for feature detection[14] and Hexicon for the analysis of deuterium incorporation. Deuterium incorporation was quantified by the mean shift of a peptide's mass centroid in triplicate measurements. The absolute mass shift difference in a peptide's "relative deuterium incorporation"[12] (ΔD_{rel}) between two states (i.e., light- vs. dark-adapted or free vs. complex-bound) was used to gauge the changes in structural changes of the corresponding region in the protein. Deuterium incorporation for individual measurements was evaluated based on the average mass increase per exchangeable amide proton (D_{norm}). Since also not corrected for back-exchange this measure gives an indication of regions with above average deuterium uptake and hence increased exchange kinetics compared to stable secondary structure elements characterized by less exchange.

Importantly, HDX data originate from an ensemble measurement which can not distinguish between asymmetric elements as would be observed in an AppA–$PpsR_2$ complex. Since the AppA-binding site is oriented to one face of the N–Q–PAS1 dimer region, elements involved in this interaction are colored on both sides of the structure. Elements colored in dark-grey represent regions not covered by peptic fragments and in addition also include two N-terminal amino acids of all identified peptides since rapid back-exchange in these positions prevents accurate measurement of deuteration.

Details of structure refinement

The $AppA_{\Delta C}$ structure was solved by experimental SAD phasing using the AutoSol feature of PHENIX combining a high resolution (2.6 Å) native dataset with anomalous data from a different crystal to 3.9 Å. Initial fragments of secondary structure elements were automatically built and extended manually in subsequent steps of refinement. Secondary structure restraints and 3 TLS groups per protomer were included for refining individual positions and B-factors. The low resolution wild-type structure was solved upon rigid-body fitting of the high resolution structure and refined using a set of dihedral restraints obtained from the high resolution model. This confirmed that the observed conformations of Trp104 and Met106 are not due to the C20S substitution. Both final models contained no outliers in the Ramachandran plot with 97 % of the residues in the favored region.

Elucidation of the PpsR ΔHTH structure was not straightforward and a detailed description will be presented elsewhere. In brief, a combination of experimental phasing (anomalous data to 5.5 Å) with molecular replacement (MR) based on shorter PpsR constructs provided a reasonable initial map for model building. Refinement initially included experimental phase information using a phased maximum-likelihood target (MLHL). In addition torsion-NCS restraints for chains A and D as well as B and C and secondary structure restraints were included together with TLS groups for the individual domains of the protein (N domain, Q-linker, PAS1 and PAS2). NCS and experimental phase restraints were omitted in the final round of refinement. Ramachandran statistics show 96.1 % of the residues in favored regions and 0.1 % outliers.

The core complex of AppA and PpsR was solved by MR based on the individual PAS domain dimers of PpsR (N and PAS1) and the four helix bundle together with the SCHIC domain of AppA. Due to the high resolution, rebuilding of elements involved in complex formation was straightforward and refinement included TLS groups for the individual domains (N domain, Q-linker, PAS1, helix bundle and SCHIC) without any additional restraints. The final model has good Ramachandran statistics with no outliers and 98.1 % the residues in the favored region.

R_{free} values[15] were computed from 5 % randomly chosen reflections not used during the refinement. 2D-plots of secondary structure elements of $AppA_{\Delta C}$ and $PpsR_{\Delta HTH}$ (Fig. 3**a** and 4**a**) were prepared by modification of automatically generated outputs obtained from the Pro-Origami server[16].

UV/Vis spectroscopy

In order to minimize spectral artifacts originating from the measuring light we used a home-built setup for addressing dark- and light-state spectra of AppA. This consists of a balanced deuterium tungsten lamp (DH-2000-BAL, Mikropack) used as measuring light source after reducing the intensity with a neutral density OD10 filter and a royal blue LED (λ_{max} = 455 nm, Doric Lenses) with variable intensity as excitation light source. Data was acquired in continuous "kinetic" mode employing a spectrograph coupled to an electron multiplying CCD detector (Andor Technology). We acquired single spectra for one second of which only selected spectra for the dark state recovery are shown. Buffer conditions for the photocycle experiments were 10 mM CHES pH 8.5, 500 mM NaCl and 5 % (w/v) glycerol.

Protein concentration determination

We estimated protein concentrations based on the calculated extinction coefficients for AppA and PpsR at 280 nm. PpsR (reduced) – 19,940 M^{-1} cm^{-1}, PpsR ΔHTH – 18,450 M^{-1} cm^{-1}, PpsR N–Q–PAS1 – 9,970 M^{-1} cm^{-1}. In the case of AppA constructs encompassing the BLUF domain, a value of ε_{280}=19,000 M^{-1} cm^{-1} was added to account for the flavin absorption and full loading with FMN was confirmed by comparison with the flavin absorbance at 445 nm based on an extinction coefficient of 12,300 M^{-1} cm^{-1}. AppA full-length (reduced) – 41,460 M^{-1} cm^{-1}, AppA Δ399 – 41,460 M^{-1} cm^{-1}, 4HB–SCHIC domain – 8,480 M^{-1} cm^{-1}.

Supplemental References

1. Masuda, S. & Bauer, C.E. AppA is a blue light photoreceptor that antirepresses photosynthesis gene expression in *Rhodobacter sphaeroides*. *Cell* **110**, 613-623 (2002).
2. Dragnea, V., Arunkumar, A.I., Lee, C.W., Giedroc, D.P. & Bauer, C.E. A Q63E *Rhodobacter sphaeroides* AppA BLUF Domain Mutant Is Locked in a Pseudo-Light-Excited Signaling State. *Biochemistry* **49**, 10682-10690 (2010).
3. Lukacs, A. et al. Photoexcitation of the Blue Light Using FAD Photoreceptor AppA Results in Ultrafast Changes to the Protein Matrix. *Journal of the American Chemical Society* **133**, 16893-16900 (2011).
4. Krissinel, E. & Henrick, K. Inference of macromolecular assemblies from crystalline state. *J Mol Biol* **372**, 774-97 (2007).
5. Waterhouse, A.M., Procter, J.B., Martin, D.M., Clamp, M. & Barton, G.J. Jalview Version 2--a multiple sequence alignment editor and analysis workbench. *Bioinformatics* **25**, 1189-91 (2009).
6. Edgar, R.C. MUSCLE: multiple sequence alignment with high accuracy and high throughput. *Nucleic Acids Research* **32**, 1792-7 (2004).
7. Kabsch, W. & Sander, C. Dictionary of protein secondary structure: pattern recognition of hydrogen-bonded and geometrical features. *Biopolymers* **22**, 2577-637 (1983).
8. Gomelsky, M. & Kaplan, S. AppA, a redox regulator of photosystem formation in *Rhodobacter sphaeroides* 2.4.1, is a flavoprotein - Identification of a novel FAD binding domain. *Journal of Biological Chemistry* **273**, 35319-35325 (1998).
9. Han, Y.C., Meyer, M.H.F., Keusgen, M. & Klug, G. A haem cofactor is required for redox and light signalling by the AppA protein of *Rhodobacter sphaeroides*. *Molecular Microbiology* **64**, 1090-1104 (2007).
10. Moskvin, O.V., Kaplan, S., Gilles-Gonzalez, M.A. & Gomelsky, M. Novel heme-based oxygen sensor with a revealing evolutionary history. *Journal of Biological Chemistry* **282**, 28740-28748 (2007).
11. Iacob, R.E. & Engen, J.R. Hydrogen exchange mass spectrometry: are we out of the quicksand? *J Am Soc Mass Spectrom* **23**, 1003-10 (2012).
12. Weis, D.D., Engen, J.R. & Kass, I.J. Semi-automated data processing of hydrogen exchange mass spectra using HX-Express. *J Am Soc Mass Spectrom* **17**, 1700-3 (2006).
13. Lou, X. et al. Deuteration distribution estimation with improved sequence coverage for HX/MS experiments. *Bioinformatics* **26**, 1535-41 (2010).
14. Renard, B.Y., Kirchner, M., Steen, H., Steen, J.A. & Hamprecht, F.A. NITPICK: peak identification for mass spectrometry data. *BMC Bioinformatics* **9**, 355 (2008).
15. Kleywegt, G.J. & Brunger, A.T. Checking your imagination: applications of the free R value. *Structure* **4**, 897-904 (1996).
16. Stivala, A., Wybrow, M., Wirth, A., Whisstock, J.C. & Stuckey, P.J. Automatic generation of protein structure cartoons with Pro-origami. *Bioinformatics* **27**, 3315-6 (2011).